Linear advection modelling: the issue of divergent flows

Vincent Guinot

ABSTRACT

Schemes for linear advection modelling in multiple dimensions on structured grids use either time-splitting or an unsplit approach for flux computation. In the case of strongly divergent flows, time-splitting introduces anisotropy in the solution whereas, with the unsplit approach, more mass than actually available may be abstracted from the computational cells, leading for instance to oscillations and sometimes instability. A simple correction for the flux, taking into account the divergence of the flow, is proposed to eliminate the problem for the unsplit approach. This correction introduces a limitation on the computational time step. An experiment carried out using a market-available software package shows that the problem above is of practical interest, and that verification procedures of modelling software should take into account simulations under non-uniform flows.

Key words | advection, multi-dimensional, stability, time-splitting

Vincent Guinot
International Institute for Infrastructural,
Hydraulics and Environmental Engineering—IHE,
PO Box 3015,
2601 DA Delft,
The Netherlands
E-mail: *vgt@ihe.nl*

INTRODUCTION

The explicit numerical solution of multi-dimensional advection problems on structured grids can be carried out using either one-dimensional algorithms with time-splitting (typically, alternate directions; Strang 1968; Yanenko 1971) or unsplit algorithms. In the first case, the multi-dimensional problem is split into a series of one-dimensional problems that are solved sequentially. The simplest possible sequence of computations, that has first-order accuracy in time (Strang 1968), is as follows (written here for the two-dimensional case):

$$\Phi^{n+1} = L_y L_x \Phi^n \tag{1}$$

where Φ^n is the discretised variable at time level m, L_x and L_y are the difference operators used to solve the one-dimensional problem in the x- and y-directions respectively, and Φ^{n+1} is the resulting variable at time level $n+1$. The problem associated with this technique is that, due to the successive use of the operators, computational solutions may become anisotropic (see tests below). The accuracy in time can be increased to the second order using the sequence (Strang 1968):

$$\Phi^{n+1} = L_y^{\frac{1}{2}} L_x L_y^{\frac{1}{2}} \Phi^n \tag{2}$$

where $L_y^{\frac{1}{2}}$ is operator L_y applied over half a time step only. A second option consists of computing all fluxes simultaneously without having recourse to time splitting:

$$\Phi^{n+1} = L_{xy} \Phi^n \tag{3}$$

where L_{xy} is an operator that solves the advection problem in the x- and y-directions simultaneously. This approach is commonly used in the engineering community (Zhao *et al.* 1994; Canson *et al.* 1999; Toro 1999). Although very simple to program, it has two major drawbacks in addition to its reduced stability: (i) the advected variable is spread artificially over the computational grid if the flow is oblique with respect to the grid, and (ii) if the flow is strongly divergent, the overlap between the domains of dependence of the edges of the computational cell may cause an artificial increase in the mass that is being taken out of the cell. Then, undesirable phenomena and non-physical results such as negative concentrations are likely to appear. The present paper aims to address the second point.

Strongly divergent flows can be encountered in a wide variety of problems, a typical example being the simulation of contaminant transport in aquifer systems in the

presence of pumping or injection wells. For the sake of clarity, two-dimensional linear advection problems will be considered, although the approach can be easily generalised to three-dimensional problems.

PROBLEM ANALYSIS AND PROPOSED SOLUTION

We examine hereafter the case of finite volume–and finite difference with control volume–type schemes. For such schemes, equation (1.3) can be rewritten as:

$$\Phi_{i,j}^{n+1} = \Phi_{i,j}^{n} + \frac{\Delta t}{\Delta x_i}\left(F_{i-\frac{1}{2},j}^{n+\frac{1}{2}} - F_{i+\frac{1}{2},j}^{n+\frac{1}{2}} \right) + \frac{\Delta t}{\Delta y_j}\left(G_{i,j-\frac{1}{2}}^{n+\frac{1}{2}} - G_{i,j+\frac{1}{2}}^{n+\frac{1}{2}} \right) \quad (4)$$

where $F_{i-\frac{1}{2},j}^{n+\frac{1}{2}}$ *and* $G_{i,j-\frac{1}{2}}^{n+\frac{1}{2}}$ are the average x- and y-fluxes respectively between time levels n and $n+1$ across the interface between cells $(i-1,j)$ and (i,j), and cells $(i,j-1)$ and (i,j) respectively, Δt is the computational time step, Δx_i and Δy_j are the widths of cell (i,j) in the x- and y-directions respectively. The semi-discretisation of the flux is in general the following:

$$F_{i-\frac{1}{2},j}^{n+\frac{1}{2}} = U_{i-\frac{1}{2},j}\Phi_{i-\frac{1}{2},j}^{n} \quad (5a)$$

$$G_{i,j-\frac{1}{2}}^{n+\frac{1}{2}} = V_{i,j-\frac{1}{2}}\Phi_{i,j-\frac{1}{2}}^{n} \quad (5b)$$

where $U_{i-\frac{1}{2},j}$ and $V_{i,j-\frac{1}{2}}$ are the average x- and y-velocities normal to the cell edge and $\Phi_{i-\frac{1}{2},j}^{n}$ and $\Phi_{i,j-\frac{1}{2}}^{n}$ are the average values at the cell edges. These values are a function of the averages $\Phi_{i,j}^{n}$ in the neighbouring cells. The simplest possible formulation consists of taking the value of Φ at an interface equal to the average value in the cell that is located upstream of this interface:

$$\Phi_{i-\frac{1}{2},j}^{n} = \Phi_{i,j}^{n} \quad \text{if } U_{i-\frac{1}{2},j} < 0 \quad (6a)$$

$$\Phi_{i-\frac{1}{2},j}^{n} = \Phi_{i-1,j}^{n} \quad \text{if } U_{i-\frac{1}{2},j} \geq 0 \quad (6b)$$

$$\Phi_{i,j-\frac{1}{2}}^{n} = \Phi_{i,j}^{n} \quad \text{if } V_{i,j-\frac{1}{2}} < 0 \quad (6c)$$

$$\Phi_{i,j-\frac{1}{2}}^{n} = \Phi_{i,j-1}^{n} \quad \text{if } V_{i,j-\frac{1}{2}} \geq 0. \quad (6d)$$

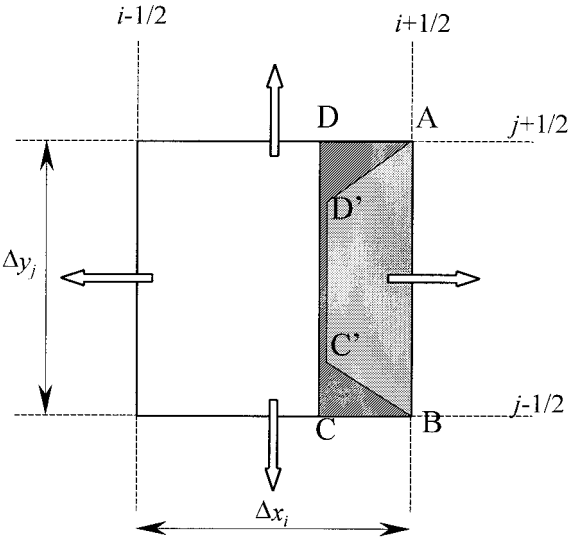

Figure 1 | Case of a strongly divergent flow. The block arrows represent the flow average over the cell edges. Rectangle (ABCD) represents the domain of dependence computed from the average velocity values. Trapezium (ABC′D′) represents the domain of dependence computed using an interpolation on the velocities.

In the case of strongly divergent flows, the use of $U_{i-\frac{1}{2},j}$ and $V_{i,j-\frac{1}{2}}$ directly in equations (5) leads to oscillations. The reason for this phenomenon is illustrated by the following simple example.

Consider the case of a cell (i,j) in which the flow is strongly divergent, so that the flow is directed outwards from the cell at all edges (see Figure 1). This is, for example, the case of an injection well in an aquifer, where the flow is radial near the well. Equations (5) implicitly assume that the streamlines are parallel near the interface and that the flow is uniform over space. According to this assumption, the dependence domain of the interface [AB] in Figure 1 (i.e. the set of points that will cross the interface [AB] during the time step) is the rectangle (ABCD). In reality, because of the divergent nature of the flow, the domain of dependence is given by the quadrangle (ABC′D′). The amount of mass, and therefore the flux, that will cross interface [AB] is therefore overestimated if equations (5) are used. Reproducing this reasoning for all edges yields the following remark: there is an overlap between the domains of dependence of the four edges of cell (i,j) because equations (5) assume that all domains of dependence are rectangles (see Figure 2).

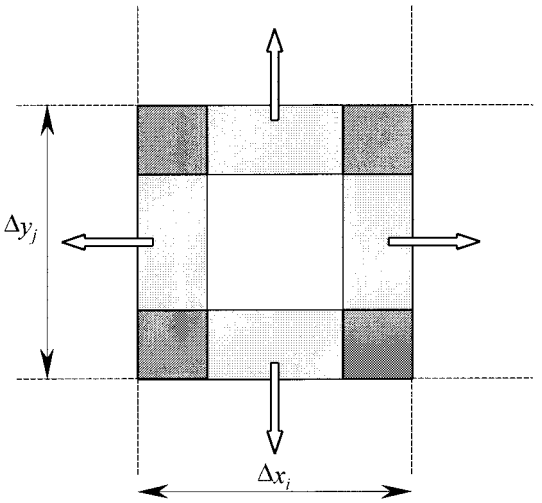

Figure 2 | Overlapping domains of dependence. Light areas: domains of dependence. Dark areas: overlapping regions.

The mass contained in the intersections between two consecutive domains (dark grey areas on the figure) will be removed twice from the cell. Consider the extreme case where the dependence domains cover half of the cell in each direction. Then the mass contained in the cell is abstracted twice instead of once. This excessive mass abstraction may lead to oscillations and, sometimes, instability.

The proposed solution consists of applying a corrective multiplication factor on the flux computed by equations (5). This multiplication factor is taken equal to the ratio between the surfaces of (ABC′D′) and (ABCD):

$$F_{i+\frac{1}{2},j} = U_{i+\frac{1}{2},j}\Phi_{i+\frac{1}{2},j}\frac{S_{\mathrm{ABC'D'}}}{S_{\mathrm{ABCD}}}. \tag{7}$$

The area of rectangle (ABCD) can be approximated with:

$$S_{\mathrm{ABCD}} = \Delta y_j U_{i+\frac{1}{2},j}\Delta t \tag{8}$$

whereas the area of (ABC′D′) is approximated as:

$$S_{\mathrm{ABC'D'}} = \tfrac{1}{2}(U^*_{i+\frac{1}{2},j}\Delta t)(\Delta y_j + \mathrm{C'D'}) \tag{9}$$

where $U^*_{i+\frac{1}{2},j}$ represents the average x-velocity over the domain of dependence. The measure of the oriented distance C′D′ is given by:

$$\mathrm{C'D'} = \Delta y_j + (V_{\mathrm{B}} - V_{\mathrm{A}})\Delta t \tag{10}$$

where V_{A} and V_{B} are the velocities at points A and B respectively. The difference between V_{B} and V_{A} can be estimated as a function of the partial derivative of the velocity with respect to y:

$$V_{\mathrm{B}} - V_{\mathrm{A}} = -\Delta y_j \left.\frac{\partial V}{\partial y}\right)_{i+\frac{1}{2},j}. \tag{11}$$

Substitution into equation (10) and then into equations (7)–(9) yields:

$$F_{i+\frac{1}{2},j} = U^*_{i+\frac{1}{2},j}\Phi_{i+\frac{1}{2},j}\left[1 - \frac{1}{2}\left.\frac{\partial V}{\partial y}\right)_{i+\frac{1}{2},j}\Delta t\right]. \tag{12}$$

Because the oriented distance C′D′ must be positive for the above formula to be valid, the time step must be lower than or equal to the limit value $\Delta t_{\max}$ given by:

$$\Delta t_{\max} = \frac{1}{\left.\dfrac{\partial V}{\partial y}\right)_{i+\frac{1}{2},j}}. \tag{13}$$

Similarly, we have:

$$G_{i,j+\frac{1}{2}} = V^*_{i,j+\frac{1}{2}}\Phi_{i,j+\frac{1}{2}}\left[1 - \frac{1}{2}\left.\frac{\partial U}{\partial x}\right)_{i,j+\frac{1}{2}}\Delta t\right]. \tag{14a}$$

$$\Delta t_{\max} = \min_{i,j}\left[\frac{1}{\left.\dfrac{\partial V}{\partial y}\right)_{i+\frac{1}{2},j}}, \frac{1}{\left.\dfrac{\partial U}{\partial x}\right)_{i,j+\frac{1}{2}}}\right] \tag{14b}$$

where $V^*_{i,j+\frac{1}{2}}$ is the average y-velocity over the domain of dependence of interface $(i, j+\frac{1}{2})$. The velocity derivatives can be estimated as follows:

$$\left.\frac{\partial V}{\partial y}\right)_{i+\frac{1}{2},j} \cong \frac{V_{i,j+\frac{1}{2}} - V_{i,j-\frac{1}{2}}}{\Delta y_j}\frac{\Delta x_{i+1}}{\Delta x_i + \Delta x_{i+1}} + \frac{V_{i+1,j+\frac{1}{2}} - V_{i+1,j-\frac{1}{2}}}{\Delta y_j}\frac{\Delta x_i}{\Delta x_i + \Delta x_{i+1}} \tag{15a}$$

$$\left.\frac{\partial U}{\partial x}\right)_{i,j+\frac{1}{2}} \cong \frac{U_{i+\frac{1}{2},j} - U_{i-\frac{1}{2},j}}{\Delta x_i}\frac{\Delta y_{j+1}}{\Delta y_j + \Delta y_{j+1}} + \frac{U_{i+\frac{1}{2},j+1} - U_{i-\frac{1}{2},j+1}}{2\Delta x_i}\frac{\Delta y_j}{\Delta y_j + \Delta y_{j+1}}. \tag{15b}$$

The velocity U^* is estimated as the ratio of the height H of the trapezium (ABC′D′) to the time step Δt. The height of

the trapezium is estimated using a first-order Taylor series expansion:

$$\begin{aligned} H &= -\int_0^{\Delta t} U(x,t)\mathrm{d}t \cong -\int_0^{\Delta t}\left[U_{i+\frac{1}{2},j} + \frac{\partial U}{\partial x}(x - x_{i+\frac{1}{2}})\right]\mathrm{d}t \\ &= -U_{i+\frac{1}{2},j}\,\Delta t + \int_0^{\Delta t}\frac{\partial U}{\partial x}(x - x_{i+\frac{1}{2}})\mathrm{d}t \\ &\cong -U_{i+\frac{1}{2},j}\,\Delta t + \int_0^{\Delta t}\frac{\partial U}{\partial x}U_{i+\frac{1}{2},j}t\mathrm{d}t \\ &= -U_{i+\frac{1}{2},j}\,\Delta t + \frac{\partial U}{\partial x}U_{i+\frac{1}{2},j}\frac{\Delta t^2}{2}\,. \end{aligned} \tag{16}$$

By definition, H is given by:

$$H = -U^*_{i+\frac{1}{2},j}\Delta t. \tag{17}$$

Substituting equation (16) into equation (17) gives:

$$U^*_{i+\frac{1}{2},j} = U_{i+\frac{1}{2},j}\left[1 - \frac{\Delta t}{2}\left.\frac{\partial U}{\partial x}\right)_{i+\frac{1}{2},j}\right]. \tag{18}$$

The derivative $\partial U/\partial x$ is approximated by:

$$\left.\frac{\partial U}{\partial x}\right)_{i+\frac{1}{2},j} = 2\,\frac{U_{i+\frac{3}{2},j} - U_{i-\frac{1}{2},j}}{\Delta x_i + \Delta x_{i+1}}\,. \tag{19}$$

Another time step limitation now has to be introduced: the two domains of dependence issuing from interface $(i-\frac{1}{2}, j)$ and $(i+\frac{1}{2}, j)$ should not intersect, and similarly for the domains of dependence in the y-direction issuing from $(i, j-\frac{1}{2})$ and $(i, j+\frac{1}{2})$. Therefore the following conditions should be satisfied:

$$(U^*_{i+\frac{1}{2},j} - U^*_{i-\frac{1}{2},j})\Delta t \le \Delta x_i \tag{20a}$$

$$(V^*_{i,j+\frac{1}{2}} - V^*_{i,j-\frac{1}{2}})\Delta t \le \Delta y_j\,. \tag{20b}$$

These conditions can be rewritten as:

$$\left[\left.\frac{\partial U}{\partial x}\right)_{i-\frac{1}{2},j} - \left.\frac{\partial U}{\partial x}\right)_{i+\frac{1}{2},j}\right]\Delta t^2 + (U_{i+\frac{1}{2},j} - U_{i-\frac{1}{2},j})\Delta t - \Delta x_i \le 0 \tag{21a}$$

$$\left[\left.\frac{\partial V}{\partial y}\right)_{i,j-\frac{1}{2}} - \left.\frac{\partial V}{\partial y}\right)_{i,j+\frac{1}{2}}\right]\Delta t^2 + (V_{i,j+\frac{1}{2}} - V_{i,j-\frac{1}{2}})\Delta t - \Delta y_j \le 0\,. \tag{21b}$$

Now focus on condition (21a) only. If, for a given interface $(i+\frac{1}{2}, j)$, it is already satisfied by the current time step, no further reduction is necessary. If it is not, two cases must be considered:

(1) $\partial U/\partial x)_{i-\frac{1}{2},j} = \partial U/\partial x)_{i+\frac{1}{2},j}$, in which equation (21a) is only a first-degree equation and the reduced time step is given by:

$$\Delta t = \frac{\Delta x_i}{U_{i+\frac{1}{2},j} - U_{i-\frac{1}{2},j}}\,. \tag{22}$$

(2) $\partial U/\partial x)_{i-\frac{1}{2},j} \neq \partial U/\partial x)_{i+\frac{1}{2},j}$, in which case a second-degree equation in Δt must be solved. The only possible root is the positive one:

$$\Delta t = \tau_1 + \tau_2 \tag{23a}$$

$$\tau_1 = \frac{1}{2}\,\frac{U_{i+\frac{1}{2},j} - U_{i-\frac{1}{2},j}}{\left.\frac{\partial U}{\partial x}\right)_{i+\frac{1}{2},j} - \left.\frac{\partial U}{\partial x}\right)_{i-\frac{1}{2},j}} \tag{23b}$$

$$\tau_2 = \frac{1}{2}\,\frac{\sqrt{4\tau_1^2 + \Delta x_i\left[\left.\frac{\partial U}{\partial x}\right)_{i+\frac{1}{2},j} - \left.\frac{\partial U}{\partial x}\right)_{i-\frac{1}{2},j}\right]}}{\left.\frac{\partial U}{\partial x}\right)_{i+\frac{1}{2},j} - \left.\frac{\partial U}{\partial x}\right)_{i-\frac{1}{2},j}}\,. \tag{23c}$$

The final formula for the fluxes is:

$$F_{i+\frac{1}{2},j} = U_{i+\frac{1}{2},j}\Phi_{i+\frac{1}{2},j} \times\left[1 - \frac{\Delta t}{2}\left.\frac{\partial U}{\partial x}\right)_{i+\frac{1}{2},j}\right]\left[1 - \frac{\Delta t}{2}\left.\frac{\partial V}{\partial y}\right)_{i+\frac{1}{2},j}\right] \tag{24a}$$

$$G_{i,j+\frac{1}{2}} = V_{i,j+\frac{1}{2}}\Phi_{i,j+\frac{1}{2}} \times\left[1 - \frac{\Delta t}{2}\left.\frac{\partial U}{\partial x}\right)_{i,j+\frac{1}{2}}\right]\left[1 - \frac{\Delta t}{2}\left.\frac{\partial V}{\partial y}\right)_{i,j+\frac{1}{2}}\right] \tag{24b}$$

where $\partial U/\partial x$ and $\partial V/\partial y$ are computed according to equations (15) and (19) and Δt is limited by equations (14b) and (21).

APPLICATION EXAMPLE

The proposed correction was applied to an extreme case, that is a purely divergent flow resulting from a continuous

Table 1 |

Symbol	Value	Meaning
h	10 m	Aquifer thickness
Δx	100 m	Cell size in the x-direction
Δy	100 m	Cell size in the y-direction
Q_i	4×10^5 m^3 d^{-1}	Injection rate
C_0	1 kg m^{-3}	Initial concentration (only in the injection cell)

injection. The spreading of a contaminant is studied in an aquifer of constant thickness subject to a pointwise injection of pure water. The injection well is represented using one computational cell only. The initial location of the contaminant is the injection cell, the rest of the aquifer being free from contamination. Pure water is injected at a constant rate. Table 1 below summarises the experimental parameters.

The analytical solution behaves as follows: the contaminant is spread away from the injection well in such a way that the contour lines for the concentration will form rings. The concentration in the ring decreases as time grows, because the perimeter covered by the ring becomes larger. Of course the numerical solution cannot be expected to behave exactly in this way because of the square shape of the cells, but as time grows the shapes of the contour lines are expected to become closer to circular rings.

Figure 3 displays the results obtained after 40 d with first-order (a) and second-order (b) time splitting and

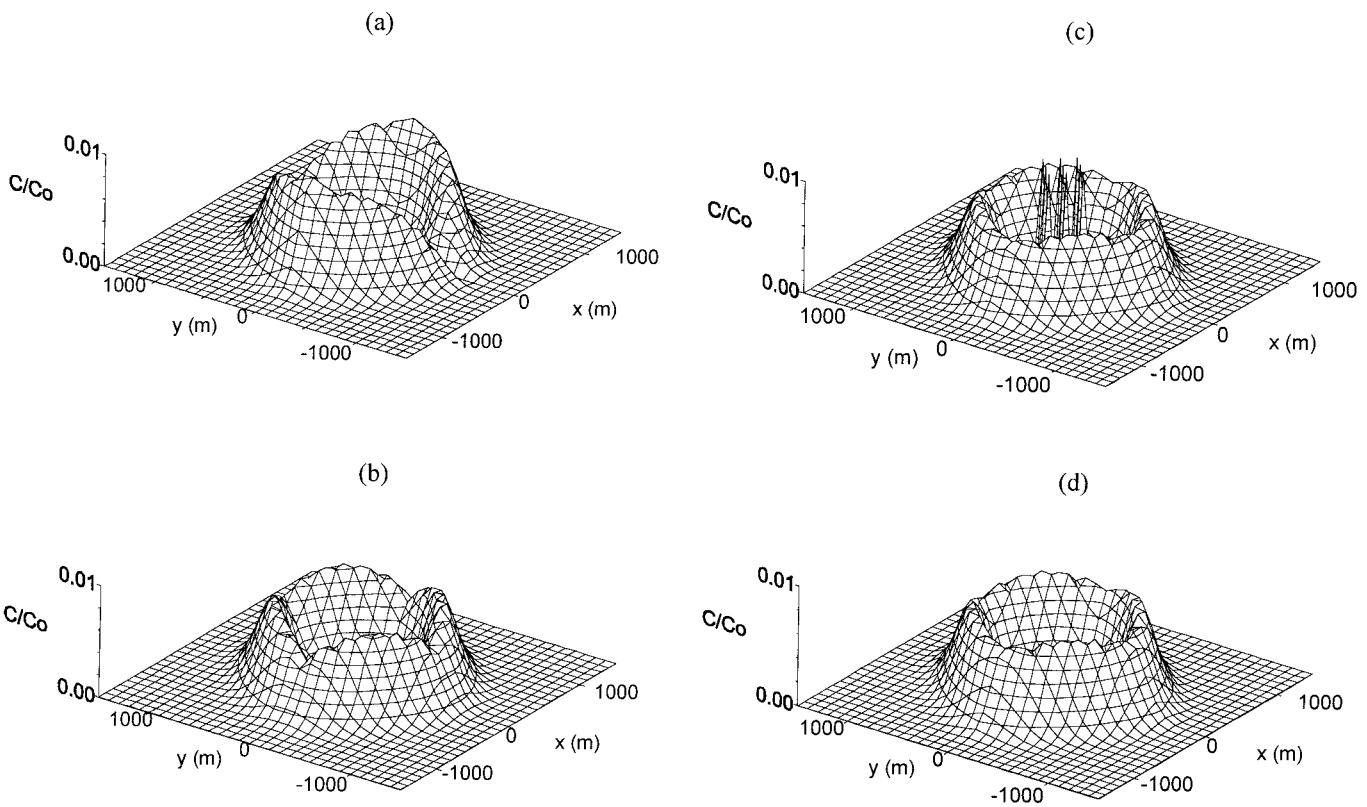

Figure 3 | Computed concentrations after 40 d for a time step Δt=0.5 d, using first-order (a) and second-order (b) time splitting and using unsplit fluxes without (c) and with (d) divergence correction. z-values have been truncated between -10^{-2} and $+10^{-2}$ for the sake of clarity of (c), where the maximum of the truncated peaks is equal to unity and the minimum is equal to $-1/3$.

using unsplit fluxes without (c) and with (d) the divergence correction for a time step Δt of 0.5 d. This value was chosen on purpose because it corresponds to the situation where the domains of dependence (ABCD) in Figure 1 cover exactly half of the cell. When fluxes are split according to equations (1), the total amount of concentration available in the injection cell is taken away by the first x-step of equation (1a). No mass is left in the cell to be taken away in the y-direction. This results in an anisotropic solution that exhibits a slot in the y-direction (Figure 3a). The use of equation (2) allows this anisotropy to be reduced to some extent (see Figure 3b), but the alignment with the main directions of the grid is obvious. When unsplit fluxes are used, the total area of the four domains of dependence associated with the four interfaces of the injection cell is equal to twice the area of the cell. Therefore, if the divergence is not accounted for, the initial mass contained in the cell is removed twice. At the next time step, the concentration in the injection cell is then the exact opposite of what it was initially, that is it oscillates between $-C_0$ and $+C_0$ from one time step to the next. These oscillations are transmitted to the neighbouring cells. Figure 3c shows the two-dimensional field for the concentration obtained after an even number of time steps. For the sake of clarity of the figure, the vertical scale has been truncated between -10^{-2} and $+10^{-2}$. Any value of the time step bigger than 0.5 d leads to an unstable behaviour, the absolute value of the concentration in the central cell growing up to infinity. In contrast, Figure 3d shows the profile obtained using the divergence correction to be free from such oscillations. In these computations, it was not necessary to apply the time step reduction of equations (13), (14), (21) and (22) because the initial value $\Delta t = 0.5$ d already complied with this condition.

Figure 4 shows the concentration fields obtained for a time step $\Delta t = 1$ d. In that case, each of the dependence domains of each interface covers the entire computational cell. When the time-splitting algorithm in equations (1) is used, the x-step removes twice the mass available from the injection cell, leaving a concentration $-C_0$. Conversely, the y-step removes twice the negative mass from the cell, bringing the concentration back to $+C_0$. The numerical solution is stable, but causes an artificial, negative concentration wave to spread in the y-direction, whereas an artificial positive one is spread in the x-direction. In addition to the lack of physical meaning, the result, as shown in Figure 4a, exhibits a strong anisotropy along the gridlines. The more accurate algorithm given by equation (2) improves the solution to some extent, but does not succeed to eliminate the artificial influence of the main directions of the grid. The reason is that for $\Delta t = 1$ d, the amount of mass that is taken away from the injection cell within $\Delta t/2$ is precisely equal to the mass available within the cell. Applying the operator $L_y^{\frac{1}{2}}$ has exactly the same consequence as applying L_y with a time step half the size and the slot that could be seen in Figure 3b can be found again in Figure 4b. If the unsplit fluxes are used without divergence correction, the concentration in the injection cell is multiplied by -3 after each time step because the dependence domains overlap four times. The numerical solution is unstable and exhibits strong oscillations (viz. Figure 4c). The values for C/C_0 shown in Figure 4c are truncated between -10^{-2} and 10^{-2} for the figure to be readable but in reality, the value in the injection cell after 40 d is higher than 10^{19}. As shown in Figure 4d, the divergence correction eliminates the spurious oscillations and instabilities. Comparison between Figures 3d and 4d shows no major difference between $\Delta t = 0.5$ d and $\Delta t = 1.0$ d.

It is worth noticing that, for $\Delta t = 1$ d, the divergence correction allows instabilities to be eliminated, although the Courant stability condition (Toro 1997, p. 556):

$$\frac{|U_{i\pm\frac{1}{2},j}|\Delta t}{\Delta x_i} + \frac{|V_{i,j\pm\frac{1}{2}}|\Delta t}{\Delta y_j} \leq 1 \quad \text{for all } i, j \tag{25}$$

is violated. This is due to the fact that the velocity field is not uniform over space. Therefore, the conclusions of the classical stability analysis (that is valid for linear equations with constant coefficients [in space and time]) do not apply here.

The expression for the analytical solution is given for further comparison. A flow particle located at a given distance r from the injection points travels at the velocity:

$$V_r = \frac{\mathrm{d}r}{\mathrm{d}t} . \tag{26}$$

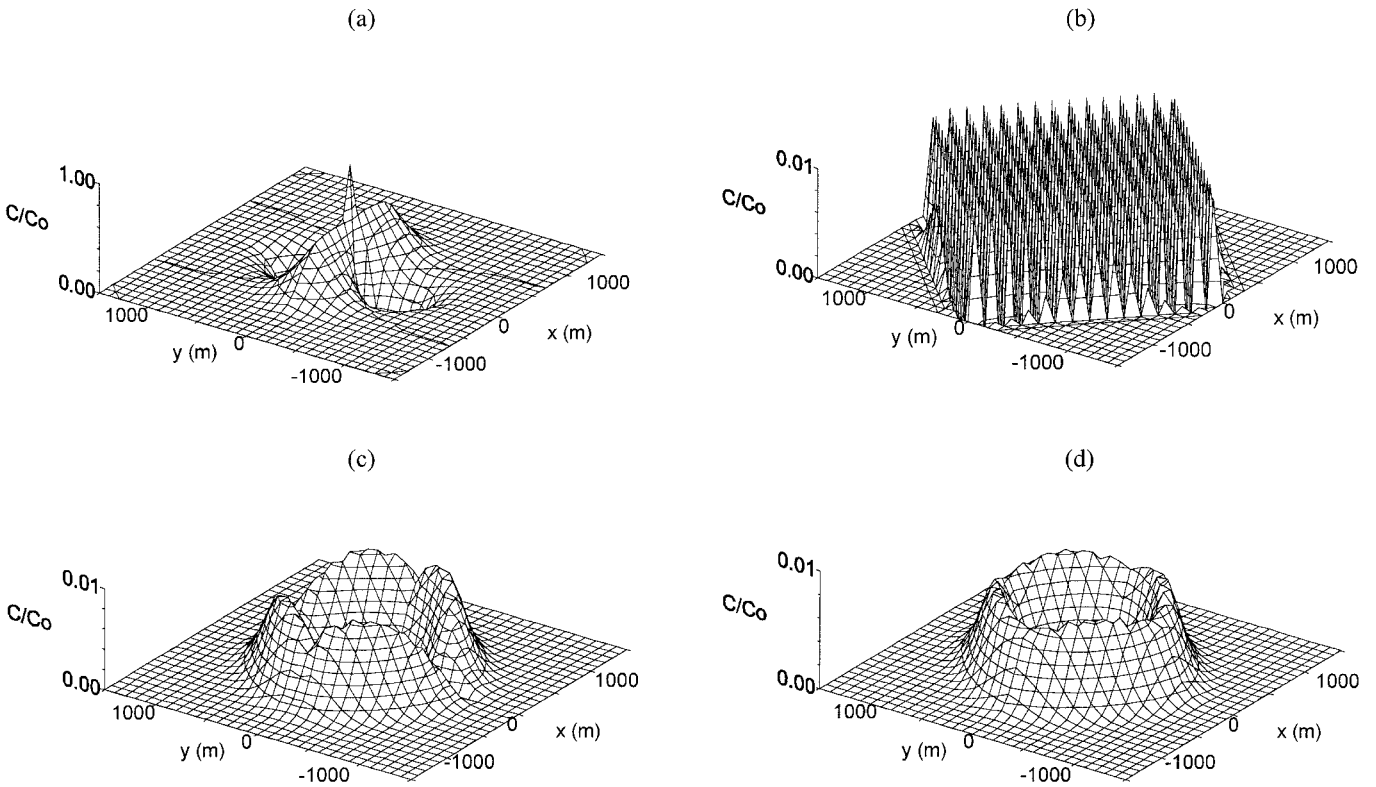

Figure 4 | Computed concentrations after 40 d for a time step $\Delta t = 1.0$ d, using first-order (a) and second-order (b) time splitting and using unsplit fluxes without (c) and with (d) divergence correction. z-values have been truncated between -10^{-2} and $+10^{-2}$ for the sake of clarity of (c). The maximum of the truncated peaks is equal to more than 10^{19}.

The radial velocity V_r is a function of the distance r to the injection point:

$$V_r = \frac{Q_i}{2\pi h r} . \tag{27}$$

Substituting equation (26) into equation (25) and solving the differential equation yields:

$$r = \sqrt{r_0^2 + \frac{Q_i}{\pi h} t} \tag{28}$$

where r_0 is the value of the distance at time $t = 0$. A circular spot of initial radius ϱ_0 will then grow into an annular region, with the following inner and outer radii r_1 and r_2:

$$r_1 = \sqrt{Q_i t / \pi h} \tag{29a}$$

$$r_2 = \sqrt{\varrho_0^2 + Q_i t / \pi h} \tag{29b}$$

which, in the present case, gives $r_1 = 713$ m and $r_2 = 715$ m. The analytical solution is shown in Figure 5. It can be seen that the numerical results, although introducing numerical diffusion due to the low accuracy of the scheme, indicate the correct location of the contaminant. Some authors (Cunge *et al*. 1980) have commented on instabilities arising from the linearisation of the equations and the use of too large time steps, although these were still in the range of stability of the linear analysis. The problem observed here, although due to large time steps, is not related to that described by Cunge *et al*. (1980) because it appears without the equations being linearised.

The present paper should not be thought of as being based on theoretical considerations alone and to have no

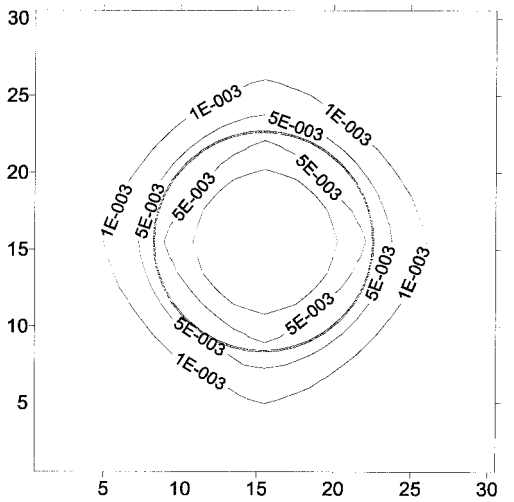

Figure 5 | Analytical (circular ring) and numerical (contour lines) solutions. The *x*- and *y*-graduations indicate the cell number.

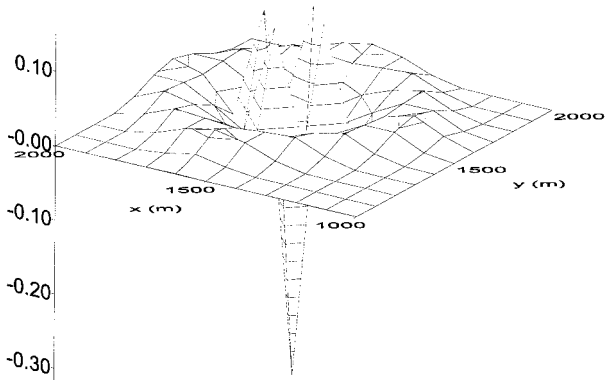

Figure 6 | Computational results obtained using a market-available software package.

practical interest. The test above was performed using a market-available code for a maximum value of the Courant number equal to unity (i.e. $\Delta t = 1$ d). Owing to lack of documentation, it cannot be guaranteed that the prescribed time step was not reduced due to additional stability constraints. However, it can be seen from Figure 6, which shows the concentration field obtained after 6 d, that oscillations and negative concentrations are still present in the solution. The amplitude of the oscillations decay very quickly with time, though they will not be completely eliminated from the solution. This example shows that, however good the performance of a given code may be under uniform or steady conditions, it may be strongly degraded when fluctuations in space (not even to talk about time) appear in the flow field. Such degradation can in general not be detected by the classical linear stability analysis, for the reasons mentioned above. Therefore verification tests should also be carried out on non-uniform and unsteady conditions.

CONCLUSION

The existence of strongly divergent flows is a factor of instability in the numerical solution of scalar advection problems. In dealing with divergent flows, the unsplit technique for flux computation exhibits a less stable, but more isotropic behaviour than time-splitting algorithms. The stability problems can be eliminated using a simple correction of the fluxes. This correction consists of redefining the velocities at the edges of the computational cells so as to avoid an overlap between the dependence domains associated with the cell interfaces. This method introduces a limitation on the computational time step. Testing the proposed method on a typical case was shown to introduce a significant improvement in the computational results as compared to both time-splitting techniques and unsplit flux without divergence correction. The appearance of instability and its elimination by the proposed solution cannot be predicted using the standard linear stability analysis. The reason for this is that the classical stability analysis is formulated for equations with constant coefficients, under uniform flow fields. A classical market-available software package is shown to exhibit poor performances on the same test, pointing to the need for more extensive verification practices in modelling software development.

NOTATION

C	computed concentration (kg m^{-3})
C_0	initial concentration (kg m^{-3})
F	flux in the x-direction (kg m^{-2} s^{-1})
G	flux in the y-direction (kg m^{-2} s^{-1})
H	height of the domain of dependence of a cell interface (m)
h	aquifer thickness (m)

L	differential operator
Q_i	injection rate ($m^3\ s^{-1}$)
r	distance to the injection point (m)
r_0	initial size of the contaminant spot (m)
r_1	inner radius of the contaminated ring (m)
r_2	outer radius of the contaminated ring (m)
t	time coordinate (s)
U	velocity in the x-direction ($m\ s^{-1}$)
U^*	modified x-velocity accounting for flow divergence ($m\ s^{-1}$)
V	velocity in the y-direction ($m\ s^{-1}$)
V^*	modified y-velocity accounting for flow divergence ($m\ s^{-1}$)
V_r	radial velocity ($m\ s^{-1}$)
x, y	space coordinates (m)
Δt	computational time step (s)
Δx	cell size in the x-direction (m)
Δy	cell size in the y-direction (m)
Φ	average value of the dependent variable over a computational cell
τ_1, τ_2	terms in the calculation of the permissible time step (s)
)	quantity is to be approximated at a given point

Subscripts

i, j	coordinates of the cell in the x- and y-directions
$i+\frac{1}{2}, j$	interface between cells i, j and $i+1, j$
$i, j+\frac{1}{2}$	interface between cells i, j and $i, j+1$
x, y	directions in which the differential operators act
max	maximum permissible value of a quantity

Superscripts

n	time level
$n+\frac{1}{2}$	averaged quantity between time levels n and $n+1$

REFERENCES

Canson, D. M., Mingham, C. G. & Ingram, D. M. 1999 Advances in calculation methods for supercritical flow in spillway channels. *J. hydraul. Engng ASCE* **125**, 1039–1050.

Cunge, J. A., Holly, F. M. Jr. & Verwey, A. 1980 *Practical Aspects of Computational River Hydraulics*. Pitman, London.

Strang, G. 1968 On the construction and comparison of difference schemes. *SIAM Jl numer. Anal.* **5**, 506–517.

Toro, E. F. 1999 *Riemann Solvers and Numerical Methods for Fluid Dynamics*, 2nd edn. Springer-Verlag, Berlin.

Yanenko, M. M. 1971. *The Method of Fractional Steps*. Springer-Verlag, New York.

Zhao, D. Z. *et al*. 1994 Finite-volume two-dimensional unsteady-flow model for river basins. *J. hydraul. Engng* (7), 863–883.